Title

Actin Cross-Linking Effector Domain of the Vibrio vulnificus F-Type MARTX Toxin Dominates Disease Progression During Intestinal Infection.

Journal

Infection and Immunity, 90(4)

Authors

Woida, Patrick

Kitts, Giordan

Shee, Stephanie

et al.

Publication Date

2022-04-21

DOI

10.1128/iai.00627-21

Peer reviewed

AMERICAN SOCIETY FOR MICROBIOLOGY | Infection and Immunity®

MOLECULAR PATHOGENESIS

Actin Cross-Linking Effector Domain of the *Vibrio vulnificus* F-Type MARTX Toxin Dominates Disease Progression During Intestinal Infection

Patrick J. Woida,[a]* Giordan Kitts,[b] Stephanie Shee,[a] Adam Godzik,[c] Karla J. F. Satchell[a]

[a]Department of Microbiology-Immunology, Northwestern University Feinberg School of Medicine, Chicago, Illinois, USA
[b]Department of Microbiology and Environmental Toxicology, University of California at Santa Cruz, Santa Cruz, California, USA
[c]Riverside School of Medicine, University of California, Riverside, California, USA

ABSTRACT *Vibrio vulnificus* is an opportunistic pathogen that causes gastroenteritis and septicemia in humans. The *V. vulnificus* multifunctional-autoprocessing repeats-in-toxin (MARTX) toxin is a pore-forming toxin that translocates multiple functionally independent effector domains into target cells and an essential virulence factor for fatal disease. The effector repertoire delivered and thus the mechanism of action of the toxin can differ dramatically across *V. vulnificus* isolates. Here, we utilize a strain of *V. vulnificus* that carries an F-type MARTX toxin that delivers an actin cross-linking domain (ACD) and four other effector domains. We demonstrate that ACD is the primary driver of virulence following intragastric infection and of bacterial dissemination to distal organs. We additionally show that ACD activates the transcription of intermediate early response genes in cultured intestinal epithelial cells (IECs). However, the genes activated by ACD are suppressed, at least in part, by the codelivered Ras/Rap1-specific endopeptidase (RRSP). The transcriptional response induced by strains translocating only RRSP results in a unique transcriptional profile, demonstrating that the transcriptional response to *V. vulnificus* is remodeled rather than simply suppressed by the MARTX toxin effector repertoire. Regardless, the transcriptional response in the intestinal tissue of infected mice is dominated by ACD-mediated induction of genes associated with response to tissue damage and is not impacted by RRSP or the three other effectors codelivered with ACD and RRSP. These data demonstrate that while other effectors do remodel early intestinal innate immune responses, ACD is the dominant driver of disease progression by ACD$^+$ *V. vulnificus* during intestinal infection.

KEYWORDS RNA-seq, *Vibrio vulnificus*, actin, intestinal epithelial cells, mouse, toxins

Vibrio vulnificus is an obligate halophile bacterium that is normally found in warm estuarine waters (1). However, *V. vulnificus* can cause severe gastroenteritis when contracted from eating raw oysters or other contaminated seafood (2). These infections can progress to primary septicemia, especially if patients have pre-existing factors, such as liver cirrhosis, hemochromatosis, or other immunocompromising conditions. While *V. vulnificus* infections are not common, with an estimated 100 cases per year in the United States (3), they have a case-fatality rate of up to 50% in primary septicemia cases and are responsible for 95% of all seafood-related deaths in the United States (1). *V. vulnificus* infections are on the rise with a 78% increase in infections between 1995 and 2006 in the US, with most cases occurring in coastal regions along the Gulf of Mexico (4, 5). However, incidences are expected to increase in northern latitudes, specifically the north Atlantic coast, as water temperatures rise due to global warming (6–9). Climate change is also expected to increase the geographic diversity of *V. vulnificus*. In the past 15 years, *V. vulnificus* has emerged in the North Atlantic and the Southern North Sea surrounding Denmark, Norway, and the eastern

Editor Manuela Raffatellu, University of California San Diego School of Medicine

Address correspondence to Karla J. F. Satchell, k-satchell@northwestern.edu.

*Present address: Patrick J. Woida, Department of Biology, Massachusetts Institute of Technology, Cambridge, MA.

The authors declare no conflict of interest.

Received 23 November 2021
Returned for modification 15 December 2021
Accepted 8 February 2022
Published 7 March 2022

A

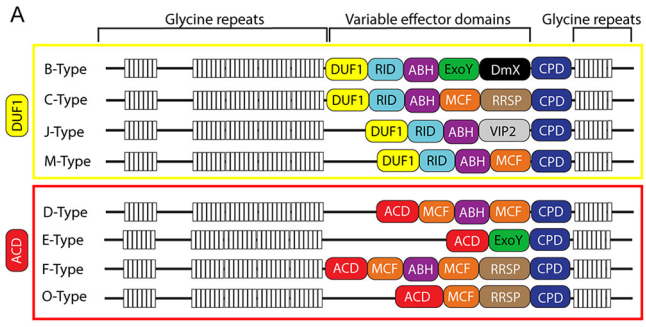

B

Strain Name	Active Effectors	Inactive/Looped Out Effectors	Schematic of Modified Effector Repitoire
98-783-DP-A1 Wild type (WT)	All active effectors	None	ACD MCF ABH MCF RRSP CPD
PWV1	MCF, ABH, and RRSP	ACD	ACD(E1990A) MCF ABH MCF RRSP CPD
PWV2	ACD, MCF, and ABH	RRSP	ACD MCF ABH MCF RRSP(H3920A) CPD
PWV3	MCF and ABH	ACD and RRSP	ACD(E1990A) MCF ABH MCF RRSP(H3920A) CPD
PWV4	ACD and RRSP	MCF and ABH	ACD ▼ΔABH-MCF MCF(C3241A) RRSP CPD
PWV5	RRSP	ACD, MCF, and ABH	ACD(E1990A) ▼ΔABH-MCF MCF(C3241A) RRSP CPD
PWV6	ACD	MCF, ABH, and RRSP	ACD ▼ΔABH-MCF MCF(C3241A) RRSP(H3920A) CPD
PWV7	None (Pore only)	All effectors inactivated	ACD(E1990A) ▼ΔABH-MCF MCF(C3241A) RRSP(H3920A) CPD
PWV8	No effectors and no pore	No effectors and no pore	MARTX toxin null strain

FIG 1 Characterized *V. vulnificus* toxinotypes and mutants used in this study. (A) MARTX toxinotypes are categorized into two groups based on a common effector in the first position: the DUF1+ toxin types (yellow box) and the ACD+ toxin types (red box). DUF1, domain of unknown function in the first position; ACD, actin cross-linking domain; MCF, Makes caterpillars floppy-like domain; ABH, alpha-beta hydrolase domain; RID, Rho inactivation domain; ExoY, Exoenzyme Y-like domain; DmX, DomainX; VIP2, vegetative insecticidal 2 homology domain; RRSP, Ras/Rap1 specific endopeptidase (53). The F-type toxin used in this study is shown at the bottom. (B) The F-type toxin in the wild-type (WT) strain 98-783-DP-A1 and the isogenic mutant derivatives created for this study. Catalytic inactive mutants are designated by X. Black triangles indicate deletion of the ABH-MCF domain. 98-783-DP-A1 plus PWV1 to -3 and PWV4 to -7 create two distinct isogenic sets with isogenic mutations in ACD and RRSP, with and without active MCF-ABH-MCF module.

coast of the United Kingdom (7). Therefore, there is a critical need to understand how *V. vulnificus* causes disease as new populations are put at risk of this severe infection.

A major virulence factor that contributes to the lethality of *V. vulnificus* is the multifunctional-autoprocessing repeats-in-toxin (MARTX) toxin (10). MARTX toxins induce epithelial cell damage (11) and are required for dissemination of the infection from the intestines to cause fatal sepsis (12). MARTX toxins are secreted as large single polypeptides that contain conserved N- and C-terminal glycine-rich repeat regions that flank a variable effector domain region and a conserved cysteine protease domain (CPD) (Fig. 1A) (13). During infection, the N- and C-terminal glycine-rich repeat regions form a pore in the host cell membrane to translocate the central effector domain region and the CPD into the host cell cytosol (13, 14). Once in the cytosol, CPD binds to inositol hexakisphosphate to activate CPD autoproteolytic activity (15–17). CPD then processes the multiple effector domains from the main holotoxin and releases them into the cytosol to perform their own independent functions (18).

MARTX toxins of *V. vulnificus* ($MARTX_{Vv}$) can carry anywhere from 2 to 5 of the 10 known MARTX effector domains (13). Novel arrangements of these effectors can arise due to horizonal gene transfer followed by homologous recombination within the gene encoding the MARTX toxin (*rtxA1*) (13). While the overall combination of effectors may vary, all sequenced MARTX toxins of *V. vulnificus* contain either a domain of unknown function in the first position (DUF1) effector (also known as RtxA1-D2 [19]), or an actin cross-linking domain (ACD) as

the first effector (13). Therefore, the known combinations of the *V. vulnificus* MARTX effector repertoires can be classified into two groups of toxin types: DUF1$^+$ B-, C-, J-, and M-type toxins; and ACD$^+$ D-, E-, and F-type toxins (Fig. 1A) (13, 20). Strains with different toxin types have varying virulence potentials, suggesting that changes in MARTX effector repertories alter virulence potential. While studies have been conducted on virulence potential and the impact of effector combinations with the more common DUF1$^+$ strains (20–23), few have been conducted with the rarer ACD$^+$ strains (23).

The ACD is a cytopathic MARTX effector domain that introduces covalent cross-links between the side chains of Lys-50 and Glu-270 in G-actin monomers (24). Serial reactions result in dimers, trimers, and higher order multiples that cannot be assembled into filamentous actin, and thus the actin cytoskeleton eventually collapses (25). An ACD effector domain also typifies the MARTX toxin of *Vibrio cholerae* (26, 27). We recently showed that the covalent cross-linking of actin, and the resulting damage to the cytoskeleton induced by the *V. cholerae* MARTX toxin, functions as a damage-associated molecular pattern (DAMP) that triggers an innate immune response in IECs (28). However, the Rho GTPase inactivation domain (RID), which inactivates Rho GTPases, and the α/β-hydrolase domain (ABH), which cleaves phosphotidylinositol-3-phosphate, are naturally codelivered with ACD on the *V. cholerae* MARTX toxin, to suppress the ACD-induced inflammatory response (28). The *V. vulnificus* ACD$^+$ D-type MARTX toxin is known to induce an early robust cytokine storm in the intraperitoneal model of infection (23). We speculated that other *V. vulnificus* ACD$^+$ MARTX toxins might also cause significant damage and inflammation when colonizing the surface of IECs and that, similar to *V. cholerae*, this inflammatory response may be modulated by other codelivered effector domains. No strain of *V. vulnificus* has been identified to carry ACD in combination with both RID and ABH. However, we speculated that *V. vulnificus* could utilize other effectors to counteract innate immune signaling in the absence of RID and ABH. Specifically, we have recently suggested that innate immune responses could be suppressed by the RAS/RAP1 specific endopeptidase (RRSP), which cleaves RAS and RAP1 GTPases (29–31).

In this study, we tested whether an F-type MARTX toxin, specifically the ACD, is essential for virulence following intragastric (IG) infection, and whether different combination of effectors modulate the proinflammatory response to *V. vulnificus*. We demonstrate that ACD is the primary driver of virulence and dissemination to distal organs in an IG model of infection. We further show that the transcriptional response to bacterial challenge in cultured IECs is distinct when ACD is alone compared to that when it is combined with RRSP. However, during infection, ACD activity in the intestine overwhelms the system such that suppression of ACD-induced gene expression by other codelivered effector domains has little overall impact on late-stage expression of inflammatory markers or on the frequency of survival, but it does reduce the time to death. Thus, our data reveal that co-introduction of ACD with other effector domains may impact the severity and decrease the time to lethality of IG and septic infection, but they further reveal that ACD is a primary driver of disease for *V. vulnificus* carrying an ACD$^+$ F-type toxin.

RESULTS

***V. vulnificus* 98-783-DP-A1 MARTX toxin has five effector domains.** The *rtxA1* gene of the MARTX toxin of *V. vulnificus* 98-783-DP-A1 was originally sequenced by the primer walking method and was annotated as carrying three effector domains (20). This previously reported partial sequence of *rtxA1* spanning only the effector domain region (20) was analyzed to generate all constructs for this study. A whole-genome sequence of 98-783-DP-A1 was conducted later in this study (NCBI accession no. JAJJIE000000000). Analysis of the full-length gene revealed that the *rtxA1* gene and the encoded MARTX toxin in this strain was much longer than expected. Reannotation revealed that 98-783-DP-A1 carries an F-type toxin (Fig. 1A and B). This arrangement, previously reported in strain FORC_009, has five effectors, including an ACD and RRSP, but also two copies of the Makes caterpillar floppy-like effector domain (MCF), which undergoes self-cleavage (32) to induce Golgi disruption (33) and apoptosis (34), and an ABH domain, which cleaves phosphatidylinositol-3-phosphate (35). The effector domain arrangement is organized

linearly as ACD-MCF-ABH-MCF-RRSP (Fig. 1A and B). The exact duplication of the *mcf* nucleotide sequence that encodes the MCF domain caused us to miss the duplication by the original primer walking method when the sequence was joined where the *mcf* gene sequences overlapped. Interestingly, this also caused misassembly of the whole-genome reads, resulting in the gene having a truncated *rtxA1* or the three effector domain arrangements in some attempts, but with a full-length *rtxA1* with the duplicated *mcf* and a single copy of *abh* in other assemblies. A previously released genome of this isolate by Sourorov et al. (NCBI Accession number DACQZU000000000.1) (36) also has the *rtxA1* gene truncated. PCR followed by sequencing of the PCR products confirmed that the toxin encoded by *rtxA1* in this strain has five effector domains (Fig. S1). A separate study is under way to consider the impact of the duplication of *mcf* on genome assembly algorithms.

The effector domains of the *V. vulnificus* 98-783-DP-A1 MARTX toxin function independently. The previously characterized glutamic acid residue required for ACD actin cross-linking was identified as E1990 (24), the cysteine residues required for MCF autoprocessing, Golgi disruption, and apoptosis are C2565 and C3241 (22, 32–34), and the histidine residue critical for RRSP cleavage of RAS and RAP1 as H3920 (31). To generate mutations that inactivate only one effector domain, we generated *in situ* site-directed mutations wherein the codons for catalytic residues were exchanged to codons for alanine within the *rtxA1* gene on the *V. vulnificus* chromosome, using homologous recombination to integrate a plasmid followed by resolution of the merodiploid with sucrose-counterselection (Fig. 1B). Unexpectedly, when mutants were generated in *mcf*, the process of integration and resolution of the merodiploid resulted in a loop out by homologous recombination between the two *mcf* copies, deleting one of the *mcf* copies and the intervening *abh* sequences and leaving a single, catalytically inactive *mcf* locus (Fig. 1B, Fig, S1). Thus, this process generated two distinct sets of isogenic mutants. The first set produces wild-type or full-length toxin with catalytic inactivation of ACD (PWV1), inactivation of RRSP (PWV2), or inactivation of both (PWV3), in a strain with the MCF-ABH-MCF module intact. The second set has the same mutations in a background with the MCF-ABH-MCF module looped out, creating a simplified toxin with a single inactive MCF (PWV4). This background was further modified to include a mutation in ACD (PWV5), a mutation in RRSP (PWV6), and the inactivation of both (PWV7). PWV7 thus produces a toxin with no active effectors. As the original sequence suggested, the toxin has only three effector domains, and the experimental design targeted only ACD, MCF, and RRSP. To keep the experimental design to a tractable number of strains for comparison (Fig. 1A), we focused our studies on possible ACD effector interplay with RRSP and considered MCF-ABH-MCF as a module, using the looped out mutant. Finally, an additional MARTX toxin-null strain was generated by inserting a kanamycin resistance cassette into the 5′-region of *rtxA1* to disrupt toxin expression, and thus produces no toxin.

The MARTX toxin glycine-rich repeat regions form a lytic pore that induces cell lysis and functions independent of the effector domains (14). Strains PWV1 to -7 all induced cell lysis of T84 IECs, as measured by lactose dehydrogenase (LDH) release, validating the introduction of single amino acid changes, and/or the loop out of the ABH-MCF module did not significantly impact overall toxin production or pore formation (Fig. S2). While PWV8 also showed a slight increase in cell lysis compared to phosphate-buffered saline (PBS)-treated cells (Fig. S2), this is probably a result of secretion of the VvhA cytolysin/hemolysin toxin, which lyses cells at later time points in the absence of *rtxA1* (11, 37). All ACD$^+$ strains showed similar actin laddering patterns in *V. vulnificus*-treated T84 IECs, confirming equivalent ACD activity (Fig. 2A). Furthermore, there was no difference in the rate of actin cross-linking between 98-783-DP-A1 and PWV6, indicating that the genetic manipulation to create the ACD+ strains did not impact toxin effector activity (Fig. S3).

A recent study revealed that CPD does not cleave between MCF and the neighboring effector on its N-terminal side (22). Instead, MCF binds to eukaryotic cell ARF family GTPases, stimulating MCF to autoprocess and separate itself from its N-terminal neighboring effector (22, 33) Inspection of the 98-783-DP-A1 toxin sequence revealed that it is missing a CPD cleavage site between ACD-MCF and thus, the successful translocation and functionality of MCF was monitored by detection of its separation from ACD. All full-length MCF-ABH-MCF-positive strains (98-783-DP-A1 and PWV1-3) showed MCF-mediated autoprocessing within treated T84

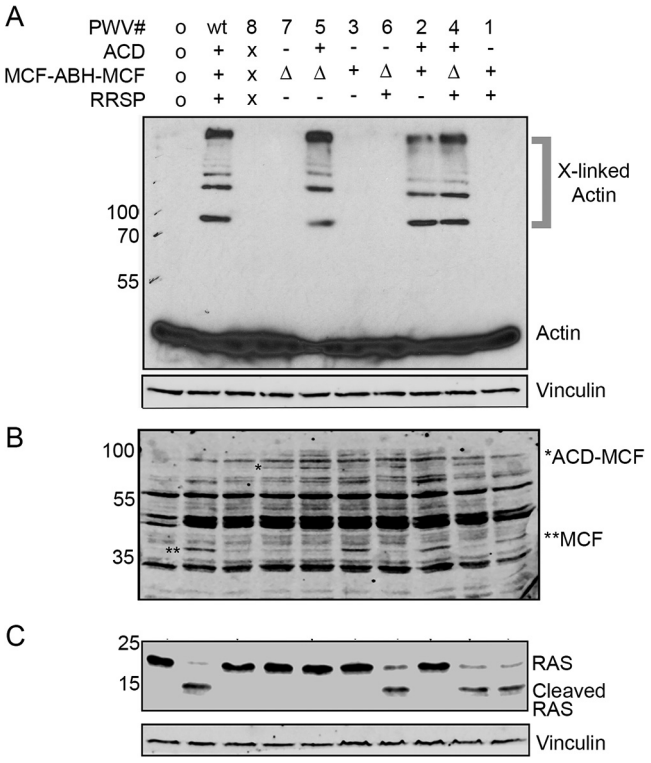

FIG 2 $MARTX_{Vv}$ toxin effectors function independently. Representative Western blots (n = 3) for (A) actin cross-linking, (B) MCF autoprocessing or (C) RAS cleavage following treatment of cells with bacteria as indicated atop panel A. Symbols used: o, no bacteria; +, effector active; –, effector catalytically inactivated; X, effector absent in toxin; Δ, MCF inactive with ABH-MCF deleted.

IECs, as indicated by the appearance of a 35-kDa band, which is consistent with the predicated size of autoprocessed MCF (32, 33) (Fig. 2B). An 80-kDa band corresponding to the ACD-MCF-tethered effectors was detected in strains with the MCF loop out (PWV4-7). An ABH-MCF band (expected to be 73 kDa) was not detected in any lane, because ABH would be released from MCF when the ABH-MCF module is intact, and the module would be absent in the looped-out strains.

Finally, all of the $RRSP^+$ strains cleaved RAS in T84 IECs, as demonstrated by the loss of the 21-kDa RAS and the appearance of the ~15-kDa processed protein (Fig. 2C). Altogether, these data support that the strains secrete functional MARTX toxins that are equivalent in activity except for the introduction of domain-specific, catalytically inactive mutations.

Effector activity of the *V. vulnificus* 98-783-DP-A1 MARTX toxin is essential for virulence in an intragastric infection model. The first activity tested by these studies was the contribution of the 98-783-DP-A1 MARTX toxin to infection. Mice were IG infected with 5×10^8 CFU of 98-783-DP-A1, PWV7, or PWV8 and monitored over 48 h for survival. Of the mice infected with the 98-783-DP-A1 toxin, 90% died within 12 h of infection (Fig. 3A). In contrast, all mice infected with either PWV7 or PWV8 survived (Fig. 3A). These studies demonstrate that the F-type MARTX toxin is essential for the virulence of *V. vulnificus* 98-783-DP-A1. Specifically, these data show that it is the catalytic activity MARTX toxin effector domains which impacts virulence potential.

Actin cross-linking dominates virulence of *V. vulnificus* 98-783-DP-A1. To examine the contribution of ACD and RRSP to virulence, at least 10 mice were infected with each strain in multiple experiments, and data were pooled for analysis. All replicate experiments included 98-783-DP-A1 and PWV7 control strains to ensure continuity across experiments. When the MCF-ABH-MCF module was present (Fig. 3B), inactivation of RRSP in strain PWV2 did not significantly impact virulence compared to that of

A

Strain Name	Active Effectors
98-783-DP-A1 WT	All active effectors
PWV1	MCF, ABH, and RRSP
PWV2	ACD, MCF, and ABH
PWV3	MCF and ABH
PWV4	ACD and RRSP
PWV5	RRSP only
PWV6	ACD only
PWV7	None (Pore only)
PWV8	Toxin null

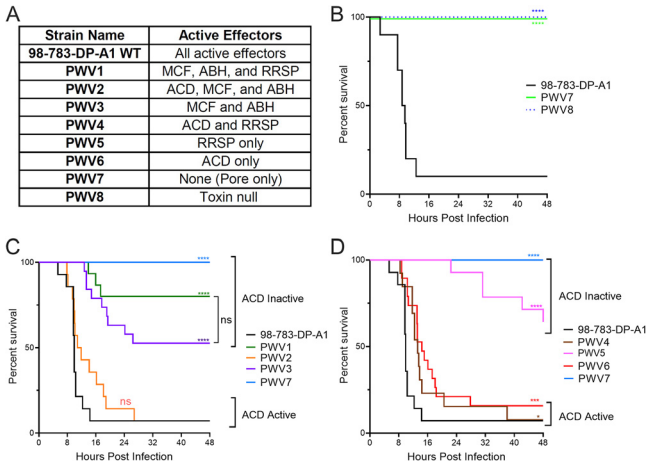

FIG 3 Survival of mice following IG infection with *V. vulnficus* MARTX effector mutants. (A) Strain designations and their corresponding active effector domains. (B,C) Mice (10 to 15 per group) were infected IG with (B) 98-783-DP-A1 or effector-free strains, (C) strains with intact MCF-ABH-MCF cassette, or (D) strains with the MCF-ABH-MCF cassette looped out and were monitored for survival over 48 h. Data were pooled from $n = 3$ experiments. Statistical comparisons done by Log-rank test compared to 98–783-DP-A1 or indicated strain. *, $P < 0.05$; ***, $P < 0.001$; ****, $P < 0.0001$; ns, nonsignificant.

the wild-type strain 98-783-DP-A1, while the loss of actin cross-linking activity in strains PWV1 and PWV3 significantly decreased virulence. There was no significant difference between PWV1 and PWV3 in survival percentage, so RRSP had minimal impact in this background with the MCF-ABH-MCF module present.

The PWV4 strain with both ACD and RRSP active, but the MCF-ABH-MCF module looped out, resulted in no change in the survival percentage imparted to 98-783-DP-A1. However, there was a reduction in the average time to death, indicating a contribution of the MCF-ABH-MCF module to virulence (Fig. 3C). Again, the presence of RRSP did not significantly impact virulence since the additional loss of RRSP did not result in significantly different virulence between strains PWV4 and PWV6. However, the loss of ACD did significantly reduce the virulence of PWV5. Here, an impact of RRSP was apparent as this strain, PWV5, with only RRSP active was more virulent than strain PWV7.

Overall, these survival data reveal that, in both the presence and absence of the MCF-ABH-MCF module, ACD dominates virulence in *V. vulnificus* 98-783-DP-A1. The MCF-ABH-MCF module resulted in 50% lethality, indicating a contribution to virulence independent of ACD and RRSP. In both contexts, RRSP does not seem to dramatically influence virulence, although RRSP alone was more virulent than a strain with no active effectors. Thus, the relative contribution of effectors to virulence is ACD $\gg$ (MCF-ABH-MCF) $>$ RRSP.

ACD independently promotes rapid dissemination from the intestines. *V. vulnificus* dissemination from the local site of infection is strongly correlated with mortality (11, 38). Further, the MARTX toxin effector domains are essential for lethal infection in strain CMCP6, specifically because they promote dissemination of the infection from the intestine to the distal organs. This dissemination occurs well ahead of the onset of acute damage due to the pore forming activity of the toxin (12). To similarly test whether the linkage of ACD with death promotes bacterial dissemination from the intestine to distal organs, spread of infection to the liver and spleen for strains 98-783-DP-A1 with all effectors, and for PWV6 with only the ACD active, was compared at 2, 5, and 7 h postinfection (hpi). At 2 hpi, mice infected with either strain showed similar CFU counts in the small intestines and little to no bacteria in the large intestines, liver, or spleen (Fig. 4A to D). At 5 hpi, both strains had disseminated to the large intestines and distal organs (Fig. 4A to D), and there were no differences in CFU count per organ between mice infected with either of the two strains at 5 or 7 hpi (Fig. 4A to D). These

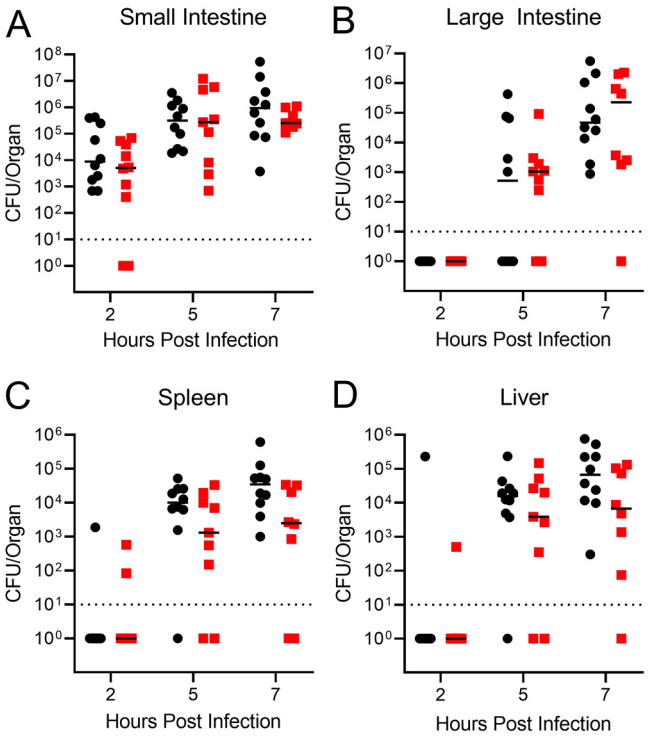

FIG 4 ACD promotes dissemination. *V. vulnificus* recovered from organs of mice inoculated IG with either 98-783-DP-A1 (black circles) or PWV6 (red squares) strains. Organs were harvested at time points indicated (n = 8 to 10). Panels recovered CFU from (A) small intestine, (B) large intestine, (C) spleen, (D) or liver. No significant differences were observed between the two strains, using either the Mann-Whitney or Welch's t test, comparing 98-783-DP-A1 with PWV6 at each time point examined.

data indicate that, among the five effector domains of 98-783-DP-A1, ACD alone is sufficient to drive bacterial dissemination from the intestine.

ACD is sufficient but not essential for dissemination. Since ACD independently promotes dissemination of strain 98-783-DP-A1, we tested whether ACD was both necessary and sufficient. To test whether ACD is necessary, dissemination was compared between 98-783-DP-A1 and PWV1, which differ only by the catalytic inactivation of the ACD. At at 7 hpi, the loss of ACD did not impact colonization of the small intestine. These data are consistent with those of prior studies, which reported that neither the *rtxA1* gene nor the conserved regions of the MARTX toxins were correlated with bacterial colonization or growth in the intestine (12). However, the loss of ACD did result in clearance of the bacterium from the large intestine in 4 out of 10 mice. There was also a statistically significant decrease in dissemination to the liver and spleen when ACD was inactivated (Fig. 5A to D).

However, these data also showed CFU recovery from both the liver and the spleen in 5 to 6 mice inoculated with PWV1, suggesting that while ACD does significantly contribute to dissemination, it is not essential (Fig. 5). This contribution to dissemination in the absence of ACD was predominantly driven by the MCF-ABH-MCF module, as there was no significant difference between PWV1 and PWV3 in dissemination at 7 hpi. (Fig. S4).

The contribution of ACD is evident in the second comparison, which was performed to directly test whether ACD is necessary (Fig. 5). There was no significant difference in CFU recovery from the intestinal tract between strain PWV6 with only ACD active compared to PWV7 with no effectors active. However, despite similar CFU in the intestine, PWV6 was significantly more likely than PWV7 to disseminate from the intestine, with only 1 to 2 mice inoculated with PWV7 showing low CFU recovery. Thus, while ACD is sufficient among the 98-783-DP-A1 effector domains to promote dissemination and is likely critical to its contribution to rapid death, ACD is not absolutely necessary, and the other effectors can work together to promote dissemination in its absence. However, the strains without

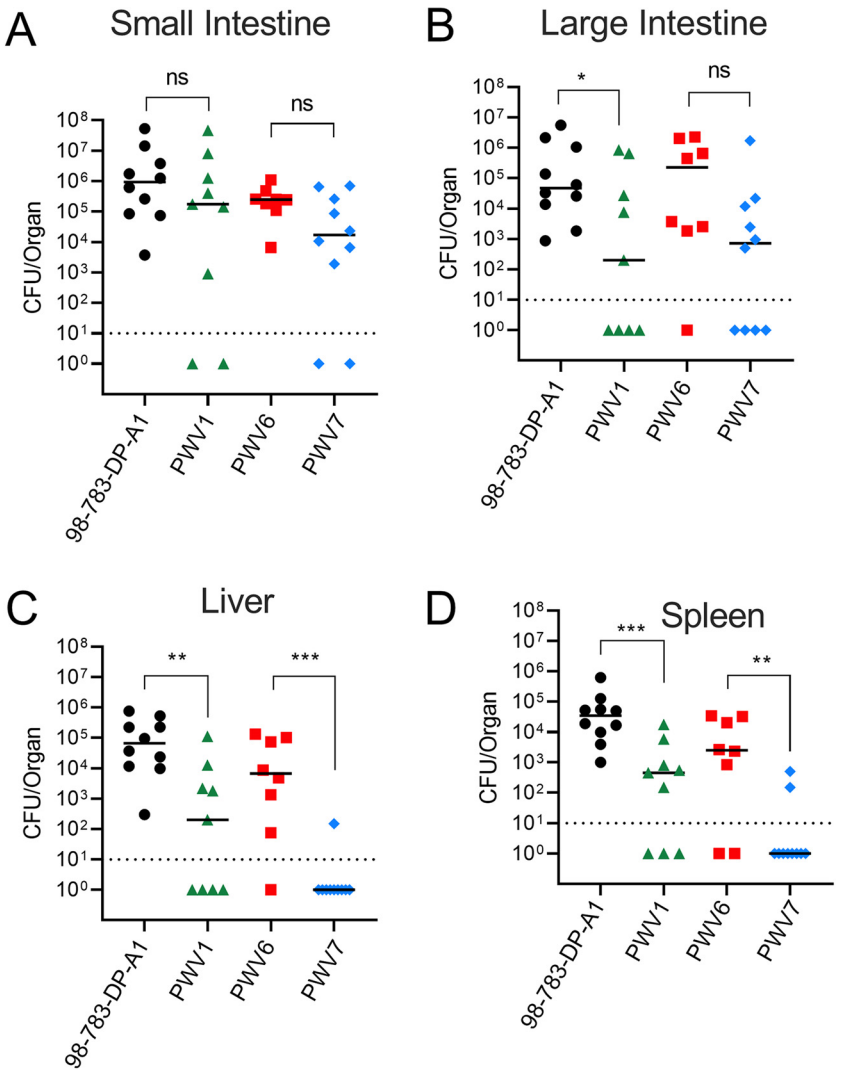

FIG 5 ACD is sufficient, but not necessary, for dissemination. *V. vulnificus* recovered from organs of mice inoculated IG with strains as indicated. Organs were harvested at 7 hpi (n = 8 to 10). Recovered CFU from (A) small intestine, (B) large intestine, (C) spleen, and (D) liver. Significant differences, indicated by brackets: *, $P < 0.05$; **, $P < 0.01$; ***, $P < 0.001$; ****, $P < 0.0001$; determined by Mann-Whitney nonparametric unpaired t tests of isogenic comparisons.

ACD were all significantly less virulent, even those with documented. These data suggest that ACD, in addition to its role in breaching the intestinal barrier, may also contribute to virulence after dissemination to distal organs.

ACD induces immediate early gene transcription in IECs. To further probe the impact of ACD on virulence, the differential transcriptional profile driven by ACD was examined. Bacteria were incubated with T84 IECs for 60 min and RNA-seq was conducted in duplicate. Differential expression compared to PBS control-treated cells was determined, with significance set at +/–1.8-fold change and an adjusted P value of <0.05 (Fig. 6A). First, the PWV7 strain with no effector domains present showed minimal changes in gene expression, with only one gene upregulated and five genes downregulated, demonstrating that the bacterial components, toxin pore, and CPD do not induce significant changes to gene expression in this time frame. Of note, the *CXCL8* gene for the neutrophil-recruiting chemokine IL-8 was significantly downregulated. The only significantly upregulated gene was *FOSB* (Fig. 6A).

This lack of differential gene expression is in stark contrast to the profile of the ACD-only strain PWV6 (Fig. 6A). When cells were undergoing actin cross-linking, there was upregulation of 31 genes, including immediate early gene response genes (39) such as *IER2* and *IER3*,

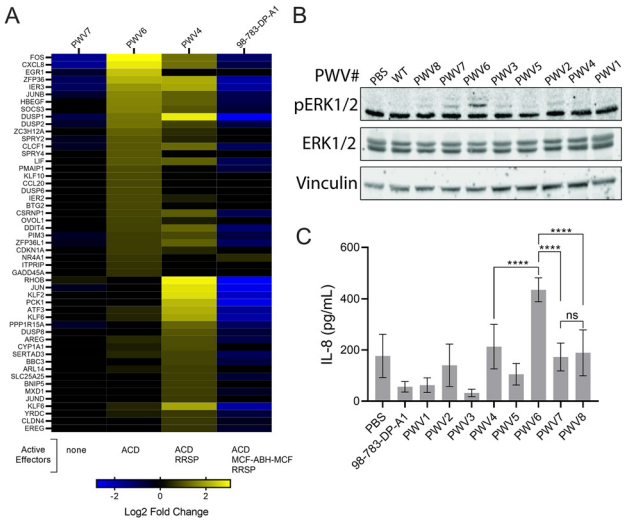

FIG 6 Effector domains differentially remodel IEC transcriptional response. (A) Heat map of differentially expressed genes identified in RNA-sequencing analysis of T84 IECs inoculated with the indicated *V. vulnificus* strains. Heat map represents statistically significant differentially expressed genes $P < 0.05$) with an >1.8 or <–1.8-fold change cutoff in duplicate experiments. (B) Representative Western blot analysis of phosphorylated ERK from T84 IECs inoculated with the indicated *V. vulnificus* strains for 60 min ($n = 3$). (C) IL-8 secretion (mean ± standard deviation, ($n = 3$) from T84 IECs inoculated with *V. vulnificus* strains. ****, $P < 0.0001$ as determined by one-way analysis of variance with Tukey's multiple-comparison test between cells treated with the indicated strains.

and the transcription factors *FOS*, *JUNB*, and *EGR1*, which control expression of proinflammatory gene expression. The chemokine gene *CXCL8* was significantly upregulated, as well as genes for the cytokines *CLCF1*, *LIF*, and *CCL20*. These data suggest that actin cross-linking induced by *V. vulnificus*, similar to previous findings for *V. cholerae* (28, 40), is a DAMP which induces inflammation in damaged epithelial cells.

Consistent with these findings, Western blots of lysates from T84 IECs treated with *V. vulnificus* with only ACD active, PWV6, showed increased phosphorylation of the MAP kinase extracellular-related kinase (ERK), which controls the expression of many immediate early genes (Fig. 6B). This upregulation was abolished when ACD was codelivered with the four other effectors on the wild-type toxin (Fig. 6B). Furthermore, when bacteria were washed out after 60 min and cells were subsequently cultured in gentamicin, cells treated with PWV6 secreted significantly more IL-8 into the medium than those treated with the toxin-free strain PWV8 (Fig. 6C). Furthermore, there was no difference between PWV7 and PWV8, indicating that IL-8 secretion is not influenced solely by the ability of the toxin to form a pore; however, the slight detection of phospho-ERK in cells treated with PWV7 and PWV8 is most likely due to lipopolysaccharide- or other bacterial pathogen-associated molecular patterns that are known to stimulate MAP kinase signaling (28). Overall, the increased phosphorylation of ERK and secretion of IL-8 were predominantly due to cellular response to actin cross-linking as the levels were significantly greater than those observed when ACD was not active in the PWV7 or PWV8 strains (Fig. 6C).

RRSP remodeled ACD-induced gene expression. We previously found that the *V. cholerae* RID silences ACD-induced gene expression. We speculated that RRSP may have a similar role based on its activity to cleave RAS, a central GTPase that controls ERK phosphorylation.

In fact, the transcriptional profile showed that most genes activated by ACD were in fact suppressed when RRSP was codelivered. Specifically, the expression of immediate early genes *EGR1*, *FOS*, *JUNB*, and *CXCL8* were reduced compared to that in the presence of ACD alone, and many of the genes upregulated by ACD were not significantly different from those of the PBS control when RRSP was also active. Interestingly, a

different set of genes was upregulated by RRSP in the presence of ACD, with the most strongly induced genes being *RHOB*, a small GTPase in the Rho family, *KLF2*, and *PCK1*. The expression profile suggests that RRSP not only blocks signaling pathways that control ACD-activated genes, but that in the absence of active RAS and RAP1, the expression of a novel set of genes is induced. Since RRSP inactivation of RAS drives loss of ERK phosphorylation (31), RRSP was shown to significantly reduce ACD-mediated stimulation of phospho-ERK, as well as IL-8 secretion (Fig. 6B and C). Co-delivery of MCF-ABH-MCF with ACD by PWV2 also reduced stimulation of phospho-ERK at 60 min (Fig. 6B). However, we cannot definitively conclude that loss of IL-8 in the MCF^+ strains was specifically due to this defect in phospho-ERK signaling, because IL-8 was measured after 22 h, at which time cells may be undergoing apoptosis due to the action of MCF (34).

One interesting finding of our data is the differential expression of the AP-1 transcription factors (Fig. 6A). AP-1 is a heterodimer, DNA-binding transcriptional activator comprised of JUN and FOS. There are multiple isoforms of these components. Interestingly, *FOSB* was upregulated by the strain with no effector domains, but it is downregulated by ACD and instead substituted by potent upregulation of *FOS*. Similarly, only *JUNB* was upregulated by ACD, whereas *JUN*, *JUNB*, and *JUND* were all upregulated by RRSP. This reveals that the transcription of AP-1 isoforms may be differentially controlled by bacterial components, ACD, and RRSP.

ACD is the primary driver of the intestinal response to infection after dissemination. As a final approach, we tested whether altered signaling may contribute to virulence outcome and if the genes *in vivo* induced by ACD would differ when delivered alone or in combination with the other effectors. To test this hypothesis, mice were mock-treated or infected with 98-783-DP-A1 or PWV6 or PWV7. RNA was extracted from the small intestines at 7 hpi and relative expression of 250 select inflammatory genes was examined using the Nanostring nCounter Inflammation Panel. Statistically significant upregulated genes in response to *V. vulnificus* 98-783-DP-A1 infection included *AGER*, *HMBG2*, *MAP3K9*, and *RAPGEF2* (Fig. 7A and B), which encode proteins in the AGER signaling pathway. *AGER* (also known as *RAGE*) encodes a surface receptor which functions in innate immune signaling, particularly in response to DAMPs. AGER interacts with exogenous ligands, including high mobility group B box proteins (HMGB1 and HMGB2), which are released from necrotic cells to stimulate initiate proinflammatory signaling. AGER specifically stimulates downstream signaling through the small GTPase RAP1 to control endothelial cell migration, through RAC GTPases to activate MAP kinases p38 and JNK, and through RAS to activate ERK. In addition to *AGER* and *HMGB2*, the gene for a G-protein exchange factor that would activate RAP1, *RAPGEF2*, and a MAP kinase that controls JNK were also upregulated. These genes were also upregulated in mice infected with the PWV6 strain which translocated only ACD without any of the other effectors active (Fig. 7A and C). These data demonstrate that the actin damage itself may be a driver of inflammation, specifically through the AGER and MAP kinase pathways, during infection.

AGER was upregulated slightly also in response to the mutant with no active effectors (Fig. 7D), but it can still cause damage through pore formation (Fig. S2). These data suggest that damage might be stimulated by other factors in addition to ACD. However, *AGER* and *HMBG2* were both significantly upregulated by PWV6 compared to PWV7 (Fig. 7E), indicating that ACD is a major driver of the response. This was further supported by a separate comparison of gene expression in response to 98-783-DP-A1 compared to PWV6, which revealed no genes that were significantly different in expression.

In addition to the AGER pathway, chemokine genes *CXCL1* and *CCL20*, which are involved in neutrophil and lymphocyte recruitment (41, 42), were upregulated by infection with both 98-783-DP-A1 and PWV6, suggesting that an immune response to clear the infection was initiated in response to the damage. Notably, these ligands in mice overlap in function with human chemokine IL-8, which is absent in mice. All other significantly regulated genes were downregulated (Fig. 7A to C). This suppression is driven by ACD, since intestines from infection groups displayed similar expression patterns (Fig. 7C). Additionally, this transcriptional response was not driven by the bacteria or the pore-forming function of the MARTX toxin,

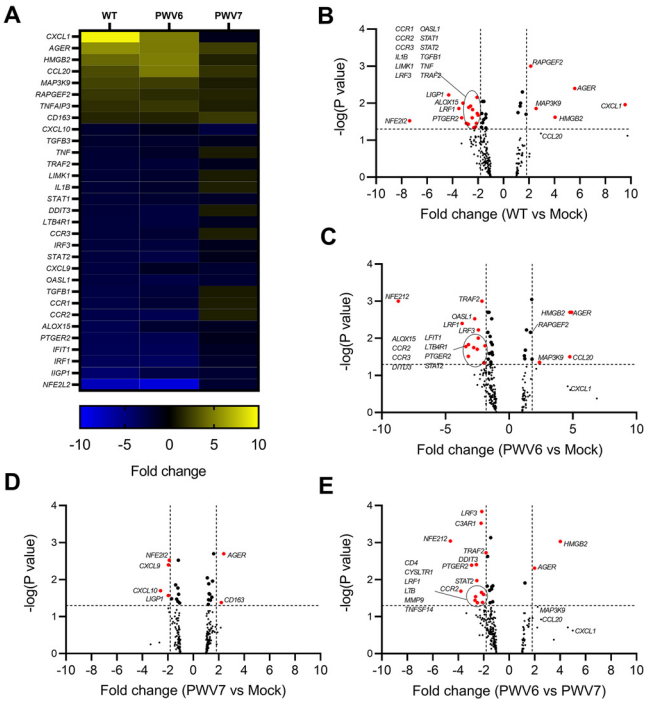

FIG 7 ACD drives late-stage transcriptional response to infection. (A) Heat map of transcriptional changes of select innate immune genes measured in resected intestinal tissue from mice infected with either WT, PWV6, or PWV7 compared to that from mock-infected mice (n = 3 mice). (B to D) Volcano plots of transcriptional responses from mice infected with (B) WT, (C) PWV6, and (D) PWV7. Large dots above the dashed 95% confidence line indicate significant data (–log[P value] $>$ 1.3, which is equivalent to $P < 0.05$). Red dots indicate significant fold change differences set at $>$1.8 or $<$–1.8, indicated by vertical dashed lines. (E) Reanalysis of gene transcription response comparing PWV6 with PWV7 *V. vulnificus* strains to show responses due solely to gain of actin cross-linking activity.

since most of the identified genes and pathways did not change in response to the effector-free strain (Fig. 7D, Table S2 and S3 in the supplemental material).

DISCUSSION

MARTX toxins are multifunctional toxins that deliver multiple cytopathic effector domains into target cells to promote virulence. However, different strains of *V. vulnificus* produce dramatically different variants of the MARTX toxin. This raises the question of the relative role of MARTX toxins during infection across different strains, and whether distinct arrangements of the toxin effectors have differential contributions to infection by different strains. In this study, we demonstrate that the F-type ACD$^+$ toxin types from *V. vulnificus* are important for virulence, as loss of function in the toxin dramatically reduced virulence. Similar findings have been shown for other *V. vulnificus* strains which secrete B-, C-, D-, F-, and M-type toxins (10, 20, 22, 23, 43), further reinforcing that across strains, MARTX toxins are essential for *V. vulnificus* virulence, even as the catalytic activity of the toxins are widely variable.

Using the IG model of infection, we established that the strains with an active ACD were more virulent than those with an inactivated ACD. This shows that ACD is the dominant virulence effector in F-type *V. vulnificus* 98-783-DP-A1. The PWV6 strain did not show any difference in small intestine colonization or dynamics of dissemination to the liver and spleen compared to the WT. These data demonstrate that ACD is sufficient among the five effector domains to promote virulence. While ACD was the dominant virulence effector, PWV6 was still slightly, yet significantly attenuated compared to 98-783-DP-A1, resulting in an increased median survival time. Inactivation of MCF autoprocessing in F-type strains has been previously

demonstrated to attenuate ACD activity due to the sequestration of ACD by unseparated MCF (22). However, replacing MCF-ABH-MCF with a single inactive MCF in our study had no impact on ACD activity (Fig. S3). Thus, the attenuation of PWV6 compared to 98-783-DP-A1 is due to the loss of the combined MCF-ABH-MCF module or RRSP activity. Analysis of their respective contributions suggests that MCF-ABH-MCF contributes to virulence when ACD is absent and enhances virulence when it is present. However, RRSP showed minimal impacts in any context except that of PWV8, a strain that produces no active effectors.

This identification of the relative contribution of effector domains in strain 98-783-DP-A1 as ACD $\gg$ (MCF-ABH-MCF) $>$ RRSP is in stark contrast to the results of previous studies, which showed that RRSP was the dominant effector of the DUF1$^+$ C-type toxin delivered by the well-studied laboratory strain CMCP6 (21). In fact, the deletion of RRSP from the toxin of CMCP6 significantly attenuated the strain, resulting in increased survival and a 50-fold change in the 50% lethal dose (LD_{50}) (20, 21). This difference is not likely due to RRSP sequence variation, as RRSP is 98% identical between the two strains and the substitutions are conservative changes located away from the functional regions for activity (31) and membrane targeting (44) (Fig. S5).

In addition, in CMCP6, we previously found no measurable contribution of MCF to overall virulence, either alone or in the presence of other effectors (21). Thus, the virulence potential of an effector domain is driven in part by the other effector domains that are present. This concept has recently been referred to in systems that translocate Type III secretion effectors as "context-dependent virulence" (45). Here, we show also that MARTX toxin effector domains are subject to context-dependent virulence potential.

One mechanism that can drive context-dependent virulence is the impact of an effector domain on inflammation. We recently showed that the ACD from the *V. cholerae* MARTX toxin induces a significant proinflammatory response that is suppressed by codelivery of RID and ABH (28). We proposed that ACD dominance in the F-type toxins may be attributed to ACD-mediated inflammation. RNA-sequencing showed that, similar to *V. cholerae*, *V. vulnificus* F-type ACD independently activated a proinflammatory response, characterized by induction of the immediate early response and expression of cytokines and chemokines such as IL-8. This response was transcriptionally abolished when ACD was codelivered with RRSP and replaced by a unique transcriptional profile. For RRSP, the transcription profile was impacted by the loss of signaling controlled by the small GTPases, RAS and RAP1. However, the impact of this intricate signaling interplay could be overwhelmed by transcriptional silencing by the MCF-ABH-MCF module, since 98-783-DP-A1 showed minimal transcriptional changes compared to mock-treated cells. The complete absence of transcriptional changes is potentially due to the nonspecific impact of downstream organelle damage by MCF on overall transcription and thus, it may not be directly related to signaling changes by MCF and/or ABH. Regardless, these data demonstrate how different effector combinations can differentially remodel the transcriptional response to infection.

Indeed, the damage induced by the MARTX toxin, specifically by ACD, was found to be the primary driver of the intestinal transcriptional response during infection. While minimal differential gene expression was observed in mice infected with an effector-free strain (Fig. 7, Table S3), the induction of genes in the AGER pathway, as well as the *CXCL1* and *CCL20* genes, indicate a response that is likely driven by cell damage with minimal impact of the codelivery of MCF-ABH-MCF-RRSP. The difference compared to our study in IECs would suggest that by 7 hpi, the damage overwhelms the response. In this case, the other effector domains may successfully delay the progression of the infection by transiently reducing inflammation, but ultimately impact only the rate of lethality, as was observed in our survival curve studies.

One surprise of the intestinal transcriptional response during infection was that many genes were suppressed despite active colonization of the gut. One explanation is that the damage induced by ACD had progressed to such an extent that many of the genes induced by it were simply no longer being expressed by 7 hpi. At this time point, our prior study of CMCP6 suggests that acute damage from pore formation and VvhA would occur at later

time points, consistent with the low response observed in strains treated with PWV8 (12). Yet this loss of gene expression is not universal, as ACD was clearly still able to stimulate expression of some chemokine expression through the damage response pathway. An alternative explanation is there is another factor produced by *V. vulnificus* 98-783-DP-A1 that drives immunosuppression in mice, and that this factor was not expressed during the 60-minute time frame of the *in vitro* IEC experiments.

The transcriptional responses observed for this F-type toxin strain were distinct from those previously reported for other *V. vulnificus* isolates. ACD$^+$ D-type toxins, which pair ACD with two copies of MCF and ABH, induced a cytokine storm after intraperitoneal infection. In contrast, DUF1$^+$ C-type toxins did not cause a cytokine storm during infection (23), yet these strains are known to be among those most frequently isolated in clinical infection. Likewise, we found that the F-type strain did not show evidence of a cytokine storm in intestinal tissues. We speculate that these differences in our findings could be related to the infection route, the time of sampling tissues, and the source of tissues for gene expression studies, indicating there may be local variation in responses depending on the resident cell types.

Overall, these data provide a preliminary model for how F-type toxin strains of *V. vulnificus* cause disease during IG infection, and further demonstrate that the key factors driving virulence are not necessarily shared across all strains of *V. vulnificus*. During early intestinal colonization, ACD cross-links actin to promote dissemination, while MCF and RRSP inactivate innate immune signaling to suppress the intestinal response to actin cross-linking. These coordinated events likely create a muted inflammatory environment during early stages of infection and enhance the rate of disease, but the effect is only transitory. By 7 hpi, there was no difference in inflammatory gene expression in response to damage and the mice continued to succumb to fatal infection. Thus, in the F-type toxins, ACD dominates virulence potential, which is in stark contrast to the dominance of RRSP in other isolates.

MATERIALS AND METHODS

Bacterial strains and plasmids. All bacterial strains and plasmids are listed in Table 1. *Escherichia coli* strains were grown on Luria-Bertani (LB) broth at 37°C and used for plasmid propagation and conjugation to modify *V. vulnificus*. *V. vulnificus* strains were grown in LB or heart infusion broth (HIB) at 30°C. When appropriate, antibiotics were added to the media at the following concentrations: rifampicin (50 μg/mL), kanamycin (50 μg/mL), and chloramphenicol (10 μg/mL for *E. coli*, 2 μg/mL for *V. vulnificus*).

Cell culture. T84 male colorectal carcinoma cells, acquired from the American Type Culture Collection (ATCC, no. CCL-248), were cultured in Dulbecco's modified Eagle's medium/nutrient mixture F-12 (DMEM/F-12) (Gibco, Thermo Fisher Scientific) with 10% (wt/vol) fetal bovine serum (FBS, Gemini Bioscience, catalog no. 900-108) and 1% (wt/vol) penicillin-streptomycin (Gibco, Thermo Fisher) at 37°C + 5% CO_2.

Generation of *V. vulnificus* MARTX toxin mutants by *in situ* site-directed mutagenesis. Fragments (gBlocks) containing alanine mutations of the identified catalytic residues of ACD, MCF, and RRSP, along with 500 bp up- and downstream from the mutations, were commercially synthesized based on the sequence determined by Kwak et al. (20). Each fragment also contained a secondary silent mutation to introduce novel Eco53K1, NotI, and PstI restriction sites near the ACD, MCF, and RRSP catalytic mutations, respectively. Sequences are listed in Table S1 in the supplemental material. Fragments were cloned into pDS132 digested with SphI (New England Biolabs, catalog no. R3182S) using Gibson Assembly (New England Biolabs, catalog no. E2611S) following manufacturers' protocols. Plasmids were confirmed by sequencing and propagated in DH5$\alpha\lambda$pir on LB supplemented with chloramphenicol.

Constructed plasmids were transformed into SM10λpir and transferred by conjugal mating to a spontaneous rifampicin resistant isolate of 98-783-DP-A1 (here used as WT). Double homologous recombinants were identified by *sacB*-counterselection as previously described (46). To confirm the recombinants gained the codon exchange, regions corresponding to the mutations were amplified by PCR using primers listed in Table S1, digested with the restriction enzyme for the introduced novel restriction site, and separated on an agarose gel. Identified recombinants were also confirmed by sequencing of the PCR product. The *rtxA1::kan* (toxin null) strain was generated by inserting a kanamycin-resistant cassette under the control of its own promoter into the repeat regions of 98-783-DP-A1 MARTX toxin using the previously constructed plasmid pKZ38 (43). The effector domain region of the 98-783-DP-A1 *rtxA1* gene (corresponding to nucleotides 5,710 to 12,018) from all strains was amplified using the primers given in Table S1 to confirm the presence of the F-type effector repertoire or the loss of *abh-mcf*.

Treatment of T84 IECs with *V. vulnificus*. *V. vulnificus* strains were grown at 30°C in LB medium supplemented with rifampicin (50 μg/mL). Overnight cultures were diluted 1:100 and grown at 30°C until exponential phase (optical density at 600 nm $\approx$ 0.5). One mL of culture was pelleted and then resuspended in PBS to a final concentration of 5×10^8 bacterial cells/mL. T84 IECs (seeded the previous day in a 12-well plate at 2×10^5 cells/well) were washed twice with 1 mL PBS and the medium was changed to FBS and antibiotic-free DMEM/F-12. Cells were then treated with *V. vulnificus* at a multiplicity of

TABLE 1 Bacterial strains and plasmids used in this study

Strain or plasmid	Description	Source or reference
V. vulnificus		
98-783-DP-A1	Isolated from market oyster, virulent in mice	43
98-783-DP-A1, Rif^R	Spontaneous Rif^r, WT[a]	This study
PWV1	98-783-DP-A1, *rtxA1-acd**	This study
PWV2	98-783-DP-A1, *rtxA1-rrsp**	This study
PWV3	98-783-DP-A1, *rtxA1-acd*-rrsp**	This study
PWV4	98-783-DP-A1, *rtxA1-mcf*-Δabh-mcf*	This study
PWV5	98-783-DP-A1, *rtxA1-acd*-mcf*-Δabh-mcf*	This study
PWV6	98-783-DP-A1, *rtxA1-mcf*-Δabh-mcf-rrsp**	This study
PWV7	98-783-DP-A1, *rtxA1-acd*-mcf*-Δabh-mcf-rrsp**	This study
PWV8	98-783-DP-A1, *rtxA1*::*kan* (MARTX null)	This study
E. coli		
DH5$\alpha\lambda$pir	Plasmid cloning	Lab stock
SM10λpir	Conjugation to *V. vulnificus*, Rif^r	Lab stock
Plasmids		
pKZ38	pDS132 with fragment of *rtxA1* with Kan^r cassette inserted in the N-term repeat region, Chl^r Kan^r	43
pPJW8	pDS132 with fragment of *rtxA1* with ACD E to A codon change, Chl^r	This study
pPJW9	pDS132 with fragment of *rtxA1* with MCF C to A codon change, Chl^r	This study
pPJW10	pDS132 with fragment of *rtxA1* with RRSP H to A codon change, Chl^r	This study

[a]WT, wild type.

infection (MOI) of 5 and spun down at 500 × *g* for 3 min to synchronize treatment. Treated cells were incubated at 37°C + 5% CO_2 for 60 min or the duration indicated.

Western blotting for cross-linked actin, MCF autoprocessing, RAS cleavage, and ERK phosphorylation. T84 IECs were treated with live bacteria as described above. After bacterial challenge, cells were washed once with 1 mL cold PBS, then scraped and harvested in 120 μL 2 × SDS loading buffer. Samples were boiled for 5 to 10 min at 95°C until they were no longer viscous. Volumes of 20 to 30 μL of each sample were separated on 10% (actin laddering), 12% (MCF autoprocessing), 15% (ERK), or 18% (RAS cleavage) SDS-polyacrylamide gels. Separated proteins were transferred to a nitrocellulose membrane and blocked in Tris-buffered Saline (TBS) with 5% powdered milk for 1 h. Membranes were washed with TBS and then incubated in primary antibody (1:1,000) in TBS + 5% bovine serum albumin (Fisher Bioreagents) overnight at 4°C. Membranes were washed in TBS and then probed in 1:10,000 IRDye800CW/680LT (LI-COR, cat no. 926-3221, 926-3211, 926-68070, and 926-6807) for 2 h in TBS + 5% milk. Membranes were washed in TBS before being imaged on a LI-COR Bioscience Odyssey Imaging System. Quantification of band density was conducted using Fiji/ImageJ. The primary antibodies used in this study were anti-actin (Sigma-Aldrich, catalog no. A2066), anti-MCF (produced from purified MCF protein; Lampire Biological Laboratories, Pipersville, PA [33]), anti-RAS (CPTC-KRAS4b-2; Developmental Studies Hybridoma Bank at the University of Iowa [31]), anti-ERK and anti-phospho-ERK (Cell Signaling Technology, catalog no. 4965S and 43372). Anti-vinculin and anti-tubulin (Cell Signaling Technology, no. 13901 and 2411) primary antibodies were used for loading controls.

Lactose dehydrogenase cytotoxicity assay. T84 IECs were treated with live bacteria as described above except bacterial treatment was performed in phenol red-free DMEM/F-12 (Gibco, Thermo Fisher) for 180 min. After bacterial treatment, medium was collected, and gentamicin was added to a volume of 100 μg/mL. Lactose dehydrogenase (LDH) activity was measured using a CytoTox 96 Non-Radioactive Cytotoxicity Assay (Promega, Madison, WI) following the manufacturer's instructions.

RNA-seq. Stranded mRNA-seq was conducted in the Northwestern University NUSeq Core Facility. Briefly, total RNA examples were checked for quality using RINs generated using an Agilent Bioanalyzer 2100. RNA quantity was determined with a Qubit Fluorometer. The Illumina TruSeq Stranded mRNA Library Preparation Kit was used to prepare sequencing libraries from 750 ng of high-quality RNA samples (RIN = 10) as recommended by the manufacturer. The Illumina NextSeq 500 Sequencer was used to sequence the libraries with the production of single-end, 75-bp reads.

The quality of DNA reads, in fastq format, was evaluated using FastQC. Adapters were trimmed and reads of poor quality or aligning to rRNA sequences were filtered. The cleaned reads were aligned to the human reference genome using STAR (47). Read counts for each gene were calculated using htseq-count (48). Normalization and differential expression were determined using the R Studio packages tidyverse (49) and DESeq2 (50). Bayesian shrinkage estimator for effect sizes was conducted using apeglm (51). The cutoff for determining significantly differentially expressed genes was an FDR-adjusted *P* value of less than 0.05 and a fold change of greater than 1.8 or less than −1.8.

IL-8 enzyme-linked immunosorbent assay. For the enzyme-linked immunosorbent assay (ELISA), 1- to 2 × 10^5 T84 IECs seeded in a 12-well tissue culture plate were treated with bacteria, as described above, for 1 h. Medium from inoculated cells was removed, cells were washed once with warm PBS, and medium was changed to DMEM/F-12 GlutaMAX medium supplemented with serum, pen-strep, and 100 μg/mL gentamicin. Cells were incubated for 37°C in the presence of 5% CO_2 for 20 h. The medium was harvested and centrifuged at 20,000 × *g* for 1 min at 4°C, then the supernatant was collected. The

concentration of IL-8 in cell medium was measured using the IL-8 Human Matched ELISA Antibody Pair Kit (Thermo Fisher, catalog no. CHC1303) following the manufacturer's instructions.

Mouse IG infections and dissemination assays. All mouse infections were conducted using protocols approved by the Northwestern Institutional Animal Care and Use Committee. Infections were performed as previously described (12, 20, 52). Briefly, female ICR mice (age 32 to 38 days) were anesthetized via intraperitoneal injection of a 100 μL cocktail of 100 μg/kg ketamine and 20 μg/kg xylazine in PBS. IG inoculations were performed using a 1-cm animal feeding tube attached to a 1-mL syringe. Mice were inoculated with 50 μL 8.5% sodium bicarbonate solution and then immediately inoculated with 50 μL of 1×10^8 CFU/mL of the indicated *V. vulnificus* strain. Bacterial doses of 5×10^6 CFU per mouse was determined based on a preliminary dose curve in which mice ($n = 5$ per dose) were challenged with doses ranging from 5×10^5 (2×10^6 CFU/mL) to 5×10^7 (1×10^9 CFU/mL). For virulence assays, mice were monitored every 2 h for the first 24 h and for 6 to 8 h for the remaining length of the experiment. All surviving mice were euthanized after 48 h, as prior studies have shown that mice surviving beyond 36 h rapidly clear the infection (11). For dissemination assays, mice were euthanized at the indicated time points and the small intestine, large intestine, liver, and spleen were harvested in 5 mL of PBS. Organs were homogenized using a hand-held homogenizer. CFU per organ was calculated by plating serial dilutions of the homogenized organs on heart-infusion broth agar supplemented with rifampicin.

Nanostring nCounter Inflammation Panel. ICR mice ($n = 3$) were mock-treated (PBS) or infected with the WT, PWV6, or PWV7 strains as described above. Mice were euthanized and intestines were harvested at 7 hpi. Small intestines were divided into 3 equal sections representing the distal, middle, and proximal regions of the small intestines before being flashed frozen. Five hundred mg of the middle section for each mouse was homogenized in 500 μL TRIzol (Thermo Fisher, catalog no. 15596026) using the Benchmark BeadBlaster Microtube Homogenizer. Homogenized tissue samples were centrifuged at 12,000 rpm for 15 min at 4°C. Next, 100 μL of chloroform was added to the harvested supernatant and incubated at room temperature for 2 min. Samples were spun down at 12,000 rpm for 15 min at 4°C. A 300-μL volume of 70% ethanol was added to the aqueous phase and RNA was extracted using the Qiagen RNeasy kit (Qiagen, catalog no. 74014) following the manufacturer's protocols. Residual gDNA was digested using the Turbo DNase kit (Thermo Fisher, no. AM2238) following the manufacturer's instructions. Relative expression of 250 selected inflammation-associated genes was examined using the nCounter Inflammation Panel (Mouse v2) performed by NanoString Technologies (Seattle, WA). All reported data were calculated using nSolver software version 4.0, available from the NanoString website (https://www.nanostring.com/). Raw data were normalized to the positive controls spiked into the sample as part of the nCounter analysis, and to housekeeping genes in the panel. Fold changes and *P* values for samples compared to those of mock-treated samples were calculated using DESeq2 in R. A separate analysis was done to compare WT with ACD, revealing no significantly different gene expression, and between ACD and the triple mutant to reveal the genes responsive to only ACD. A raw data file is provided in the supplement.

Statistical analysis. All statistical analysis and graphing of data were performed as detailed in figure legends using GraphPad Prism 8 or 9.

Data availability. The genome sequence for *V. vulnificus* 98-783-DP-A1 is deposited to NCBI GenBank as Accession number JAJJIE000000000. The RNA-seq data have been deposited in the NCBI Gene Expression Omnibus (GEO) (https://www.ncbi.nlm.nih.gov/geo/) under the accession number GSE189194. Raw read data for the transcriptome analysis in IECs and nCounter are given in Tables S2 and S3.

SUPPLEMENTAL MATERIAL

Supplemental material is available online only.

SUPPLEMENTAL FILE 1, PDF file, 1.7 MB.

SUPPLEMENTAL FILE 2, XLSX file, 0.02 MB.

SUPPLEMENTAL FILE 3, XLSX file, 0.01 MB.

ACKNOWLEDGMENTS

We thank members of the Satchell Laboratory for valuable input and technical support. We thank Kendall Kling for assistance with whole-genome sequencing of 98-783-DP-A1, and we thank Ryan Embry and Matthew Schipma of the Northwestern NUSeq core for preliminary analysis of RNA-seq data. We also thank the laboratory of Alan Hauser for the use of the Benchmark BeadBlaster Homogenizer. This work was funded by the NIH Ruth L. Kirschstein Institutional National Research Service Award Training grant in Immunology and Microbial Pathogenesis no. T32AI007476 (to P.J.W.) and by NIH grant no. R01AI092825 (to K.J.F.S.).

REFERENCES

1. Baker-Austin C, Oliver JD. 2018. *Vibrio vulnificus*: new insights into a deadly opportunistic pathogen. Environ Microbiol 20:423–430. https://doi.org/10.1111/1462-2920.13955.
2. Oliver JD. 2015. The biology of *Vibrio vulnificus*. Microbiol Spectr 3. https://doi.org/10.1128/microbiolspec.VE-0001-2014.
3. Baker-Austin C, Oliver JD. 2020. *Vibrio vulnificus*. Trends Microbiol 28:81–82. https://doi.org/10.1016/j.tim.2019.08.006.
4. Centers for Disease Control and Prevention (CDC). 2007. Preliminary FoodNet data on the incidence of infection with pathogens transmitted commonly through food: 10 states, 2006. MMWR Morb Mortal Wkly Rep 56:336–339.
5. Heng SP, Letchumanan V, Deng CY, Ab Mutalib NS, Khan TM, Chuah LH, Chan KG, Goh BH, Pusparajah P, Lee LH. 2017. *Vibrio vulnificus*: an environmental and clinical burden. Front Microbiol 8:997. https://doi.org/10.3389/fmicb.2017.00997.

6. Paz S, Bisharat N, Paz E, Kidar O, Cohen D. 2007. Climate change and the emergence of *Vibrio vulnificus* disease in Israel. Environ Res 103:390–396. https://doi.org/10.1016/j.envres.2006.07.002.
7. Vezzulli L, Grande C, Reid PC, Helaouet P, Edwards M, Hofle MG, Brettar I, Colwell RR, Pruzzo C. 2016. Climate influence on *Vibrio* and associated human diseases during the past half-century in the coastal North Atlantic. Proc Natl Acad Sci U S A 113:E5062–E5071. https://doi.org/10.1073/pnas.1609157113.
8. Baker-Austin C, Trinanes J, Taylor N, Hartnell R, Siitonen A, Martinez-Urtaza J. 2013. Emerging *Vibrio* risk at high latitudes in response to ocean warming. Nat Clim Chang 3:73–77. https://doi.org/10.1038/nclimate1628.
9. Muhling BA, Jacobs J, Stock CA, Gaitan CF, Saba VS. 2017. Projections of the future occurrence, distribution, and seasonality of three *Vibrio* species in the Chesapeake Bay under a high-emission climate change scenario. Geohealth 1:278–296. https://doi.org/10.1002/2017GH000089.
10. Lee JH, Kim MW, Kim BS, Kim SM, Lee BC, Kim TS, Choi SH. 2007. Identification and characterization of the *Vibrio vulnificus rtxA* essential for cytotoxicity *in vitro* and virulence in mice. J Microbiol 45:146–152.
11. Jeong HG, Satchell KJ. 2012. Additive function of *Vibrio vulnificus* MARTX (*Vv*) and VvhA cytolysins promotes rapid growth and epithelial tissue necrosis during intestinal infection. PLoS Pathog 8:e1002581. https://doi.org/10.1371/journal.ppat.1002581.
12. Gavin HE, Beubier NT, Satchell KJ. 2017. The effector domain region of the *Vibrio vulnificus* MARTX toxin confers biphasic epithelial barrier disruption and is essential for systemic spread from the intestine. PLoS Pathog 13:e1006119. https://doi.org/10.1371/journal.ppat.1006119.
13. Satchell KJF. 2015. Multifunctional-autoprocessing repeats-in-toxin (MARTX) Toxins of *Vibrios*. Microbiol Spectr 3. https://doi.org/10.1128/microbiolspec.VE-0002-2014.
14. Kim BS, Gavin HE, Satchell KJ. 2015. Distinct roles of the repeat-containing regions and effector domains of the *Vibrio vulnificus* multifunctional-autoprocessing repeats-in-toxin (MARTX) toxin. mBio 6:e00324-15. https://doi.org/10.1128/mBio.00324-15.
15. Sheahan KL, Cordero CL, Satchell KJ. 2007. Autoprocessing of the *Vibrio cholerae* RTX toxin by the cysteine protease domain. EMBO J 26:2552–2561. https://doi.org/10.1038/sj.emboj.7601700.
16. Lupardus PJ, Shen A, Bogyo M, Garcia KC. 2008. Small molecule-induced allosteric activation of the *Vibrio cholerae* RTX cysteine protease domain. Science 322:265–268. https://doi.org/10.1126/science.1162403.
17. Prochazkova K, Satchell KJ. 2008. Structure-function analysis of inositol hexakisphosphate-induced autoprocessing of the *Vibrio cholerae* multifunctional autoprocessing RTX toxin. J Biol Chem 283:23656–23664. https://doi.org/10.1074/jbc.M803334200.
18. Prochazkova K, Shuvalova LA, Minasov G, Voburka Z, Anderson WF, Satchell KJ. 2009. Structural and molecular mechanism for autoprocessing of MARTX toxin of *Vibrio cholerae* at multiple sites. J Biol Chem 284:26557–26568. https://doi.org/10.1074/jbc.M109.025510.
19. Kim BA, Lim JY, Rhee JH, Kim YR. 2016. Characterization of prohibitin 1 as a host partner of *Vibrio vulnificus* RtxA1 toxin. J Infect Dis 213:131–138. https://doi.org/10.1093/infdis/jiv362.
20. Kwak JS, Jeong HG, Satchell KJ. 2011. *Vibrio vulnificus rtxA1* gene recombination generates toxin variants with altered potency during intestinal infection. Proc Natl Acad Sci U S A 108:1645–1650. https://doi.org/10.1073/pnas.1014339108.
21. Gavin HE, Satchell KJF. 2019. RRSP and RID effector domains dominate virulence impact of *Vibrio vulnificus* MARTX toxin. J Infect Dis 219:889–897. https://doi.org/10.1093/infdis/jiy590.
22. Lee Y, Kim BS, Choi S, Lee EY, Park S, Hwang J, Kwon Y, Hyun J, Lee C, Kim JF, Eom SH, Kim MH. 2019. Makes caterpillars floppy-like effector-containing MARTX toxins require host ADP-ribosylation factor (ARF) proteins for systemic pathogenicity. Proc Natl Acad Sci U S A 116:18031–18040. https://doi.org/10.1073/pnas.1905095116.
23. Murciano C, Lee CT, Fernandez-Bravo A, Hsieh TH, Fouz B, Hor LI, Amaro C. 2017. MARTX Toxin in the Zoonotic Serovar of *Vibrio vulnificus* triggers an early cytokine storm in mice. Front Cell Infect Microbiol 7:332. https://doi.org/10.3389/fcimb.2017.00332.
24. Geissler B, Bonebrake A, Sheahan KL, Walker ME, Satchell KJ. 2009. Genetic determination of essential residues of the *Vibrio cholerae* actin cross-linking domain reveals functional similarity with glutamine synthetases. Mol Microbiol 73:858–868. https://doi.org/10.1111/j.1365-2958.2009.06810.x.
25. Fullner KJ, Mekalanos JJ. 2000. In vivo covalent cross-linking of cellular actin by the *Vibrio cholerae* RTX toxin. EMBO J 19:5315–5323. https://doi.org/10.1093/emboj/19.20.5315.
26. Sheahan KL, Cordero CL, Satchell KJ. 2004. Identification of a domain within the multifunctional *Vibrio cholerae* RTX toxin that covalently cross-links actin. Proc Natl Acad Sci U S A 101:9798–9803. https://doi.org/10.1073/pnas.0401104101.
27. Dolores J, Satchell KJ. 2013. Analysis of *Vibrio cholerae* genome sequences reveals unique rtxA variants in environmental strains and an *rtxA*-null mutation in recent altered El Tor isolates. mBio 4:e00624. https://doi.org/10.1128/mBio.00624-12.
28. Woida PJ, Satchell KJF. 2020. The *Vibrio cholerae* MARTX toxin silences the inflammatory response to cytoskeletal damage before inducing actin cytoskeleton collapse. Sci Signal 13:eaaw9447. https://doi.org/10.1126/scisignal.aaw9447.
29. Antic I, Biancucci M, Zhu Y, Gius DR, Satchell KJF. 2015. Site-specific processing of Ras and Rap1 Switch I by a MARTX toxin effector domain. Nat Commun 6:7396. https://doi.org/10.1038/ncomms8396.
30. Antic I, Biancucci M, Satchell KJ. 2014. Cytotoxicity of the *Vibrio vulnificus* MARTX toxin effector DUF5 is linked to the C2A subdomain. Proteins 82:2643–2656. https://doi.org/10.1002/prot.24628.
31. Biancucci M, Minasov G, Banerjee A, Herrera A, Woida PJ, Kieffer MB, Bindu L, Abreu-Blanco M, Anderson WF, Gaponenko V, Stephen AG, Holderfield M, Satchell KJF. 2018. The bacterial Ras/Rap1 site-specific endopeptidase RRSP cleaves Ras through an atypical mechanism to disrupt Ras-ERK signaling. Sci Signal 11:eaat8335. https://doi.org/10.1126/scisignal.aat8335.
32. Agarwal S, Agarwal S, Biancucci M, Satchell KJ. 2015. Induced autoprocessing of the cytopathic Makes caterpillars floppy-like effector domain of the *Vibrio vulnificus* MARTX toxin. Cell Microbiol 17:1494–1509. https://doi.org/10.1111/cmi.12451.
33. Herrera A, Muroski J, Sengupta R, Nguyen HH, Agarwal S, Ogorzalek Loo RR, Mattoo S, Loo JA, Satchell KJF. 2020. N-terminal autoprocessing and acetylation of multifunctional-autoprocessing repeats-in-toxins (MARTX) Makes caterpillars floppy-like effector is stimulated by adenosine diphosphate (ADP)-ribosylation factor 1 in advance of Golgi fragmentation. Cell Microbiol 22:e13133. https://doi.org/10.1111/cmi.13133.
34. Agarwal S, Zhu Y, Gius DR, Satchell KJ. 2015. The Makes caterpillars floppy (MCF)-like domain of *Vibrio vulnificus* induces mitochondrion-mediated apoptosis. Infect Immun 83:4392–4403. https://doi.org/10.1128/IAI.00570-15.
35. Agarwal S, Kim H, Chan RB, Agarwal S, Williamson R, Cho W, Paolo GD, Paolo GD, Satchell KJF. 2015. Autophagy and endosomal trafficking inhibition by *Vibrio cholerae* MARTX toxin phosphatidylinositol-3-phosphate-specific phospholipase A1 activity. Nat Commun 6:8745. https://doi.org/10.1038/ncomms9745.
36. Souvorov A, Agarwala R, Lipman DJ. 2018. SKESA: strategic k-mer extension for scrupulous assemblies. Genome Biol 19:153. https://doi.org/10.1186/s13059-018-1540-z.
37. Kim YR, Lee SE, Kook H, Yeom JA, Na HS, Kim SY, Chung SS, Choy HE, Rhee JH. 2008. *Vibrio vulnificus* RTX toxin kills host cells only after contact of the bacteria with host cells. Cell Microbiol 10:848–862. https://doi.org/10.1111/j.1462-5822.2007.01088.x.
38. Kashimoto T, Iwasaki C, Gojo M, Sugiyama H, Yoshioka K, Yamamoto Y, Okamura M, Susa N, Ueno S. 2015. *Vibrio vulnificus* detected in the spleen leads to fatal outcome in a mouse oral infection model. FEMS Microbiol Lett 362:fnv0005. https://doi.org/10.1093/femsle/fnv005.
39. Bahrami S, Drablos F. 2016. Gene regulation in the immediate-early response process. Adv Biol Regul 62:37–49. https://doi.org/10.1016/j.jbior.2016.05.001.
40. Ma AT, Mekalanos JJ. 2010. In vivo actin cross-linking induced by *Vibrio cholerae* type VI secretion system is associated with intestinal inflammation. Proc Natl Acad Sci U S A 107:4365–4370. https://doi.org/10.1073/pnas.0915156107.
41. Frommhold D, Kamphues A, Dannenberg S, Buschmann K, Zablotskaya V, Tschada R, Lange-Sperandio B, Nawroth PP, Poeschl J, Bierhaus A, Sperandio M. 2011. RAGE and ICAM-1 differentially control leukocyte recruitment during acute inflammation in a stimulus-dependent manner. BMC Immunol 12:56. https://doi.org/10.1186/1471-2172-12-56.
42. Klein M, Brouwer MC, Angele B, Geldhoff M, Marquez G, Varona R, Hacker G, Schmetzer H, Hacker H, Hammerschmidt S, van der Ende A, Pfister HW, van de Beek D, Koedel U. 2014. Leukocyte attraction by CCL20 and its receptor CCR6 in humans and mice with pneumococcal meningitis. PLoS One 9:e93057. https://doi.org/10.1371/journal.pone.0093057.
43. Ziolo KJ, Jeong HG, Kwak JS, Yang S, Lavker RM, Satchell KJ. 2014. *Vibrio vulnificus* biotype 3 multifunctional autoprocessing RTX toxin is an adenylate cyclase toxin essential for virulence in mice. Infect Immun 82:2148–5217. https://doi.org/10.1128/IAI.00017-14.
44. Geissler B, Ahrens S, Satchell KJ. 2012. Plasma membrane association of three classes of bacterial toxins is mediated by a basic-hydrophobic motif. Cell Microbiol 14:286–298. https://doi.org/10.1111/j.1462-5822.2011.01718.x.

45. Ruano-Gallego D, Sanchez-Garrido J, Kozik Z, Nunez-Berrueco E, Cepeda-Molero M, Mullineaux-Sanders C, Naemi-Baghshomali Clark J, Slater SL, Wagner N, Glegola-Madejska I, Roumeliotis TI, Pupko T, Fernandez LA, Rodriguez-Paton A, Choudhary JS, Frankel G. 2021. Type III secretion system effectors form robust and flexible intracellular virulence networks. Science 371:eabc9531. https://doi.org/10.1126/science.abc9531.
46. Fullner KJ, Mekalanos JJ. 1999. Genetic characterization of a new type IV-A pilus gene cluster found in both classical and El Tor biotypes of *Vibrio cholerae*. Infect Immun 67:1393–1404. https://doi.org/10.1128/IAI.67.3.1393-1404.1999.
47. Dobin A, Davis CA, Schlesinger F, Drenkow J, Zaleski C, Jha S, Batut P, Chaisson M, Gingeras TR. 2013. STAR: ultrafast universal RNA-seq aligner. Bioinformatics 29:15–21. https://doi.org/10.1093/bioinformatics/bts635.
48. Anders S, Pyl PT, Huber W. 2015. HTSeq: a Python framework to work with high-throughput sequencing data. Bioinformatics 31:166–169. https://doi.org/10.1093/bioinformatics/btu638.
49. Wickham H, Averick M, Bryan J, Chang W, McGowan L, François R, Grolemund G, Hayes A, Henry L, Hester J, Kuhn M, Pedersen T, Miller E, Bache S, Müller K, Ooms J, Robinson D, Seidel D, Spinu V, Takahashi K, Vaughan D, Wilke C, Woo K, Yutani H. 2019. Welcome to the Tidyverse. Joss 4:1686. https://doi.org/10.21105/joss.01686.
50. Love MI, Huber W, Anders S. 2014. Moderated estimation of fold change and dispersion for RNA-seq data with DESeq2. Genome Biol 15:550. https://doi.org/10.1186/s13059-014-0550-8.
51. Zhu A, Ibrahim JG, Love MI. 2019. Heavy-tailed prior distributions for sequence count data: removing the noise and preserving large differences. Bioinformatics 35:2084–2092. https://doi.org/10.1093/bioinformatics/bty895.
52. Olivier V, Queen J, Satchell KJ. 2009. Successful small intestine colonization of adult mice by *Vibrio cholerae* requires ketamine anesthesia and accessory toxins. PLoS One 4:e7352. https://doi.org/10.1371/journal.pone.0007352.
53. Woida PJ, Satchell KJF. 2018. Coordinated delivery and function of bacterial MARTX toxin effectors. Mol Microbiol 107:133–141. https://doi.org/10.1111/mmi.13875.